

Understanding radial flow fluctuations in the quark-gluon plasma via event-by-event momentum rescaling approach

Jiangyong Jia^{1,2}

¹*Department of Chemistry, Stony Brook University, Stony Brook, NY 11794, USA*

²*Physics Department, Brookhaven National Laboratory, Upton, NY 11976, USA*

(Dated: July 22, 2025)

The transverse momentum (p_T) differential radial flow fluctuation, $v_0(p_T)$, has emerged as a new probe of the quark-gluon plasma in heavy-ion collisions. I present a framework that recasts $v_0(p_T)$ as a p_T -dependent momentum rescaling function $g(p_T)$. This transformation reveals that constant rescaling ($g(p_T) = 1$) captures the main features of $v_0(p_T)$, including its characteristic rise-and-fall pattern that emerges naturally from the particle spectral shape. Analysis of ATLAS data at $\sqrt{s_{NN}} = 5.02$ TeV reveals small but significant deviations of $g(p_T)$ from unity with clear centrality dependence. This transformation converts $v_0(p_T)$ into a transparent probe of p_T -dependent dynamics: $g(p_T) < 1$ signals suppressed fluctuations while $g(p_T) > 1$ indicates enhanced fluctuations relative to global radial flow. Predictions for lower energies reveal spectral shape differences alone could generate substantial variations in $v_0(p_T)$. This framework enables direct connections between theoretical predictions and underlying physics mechanisms.

Introduction. Heavy ion collisions at RHIC and the LHC create the quark-gluon plasma (QGP), a state of matter composed of deconfined quarks and gluons. A fundamental aspect of these collisions is radial flow, representing the isotropic component of collective expansion driven by pressure gradients established in the initial stages of the collision [1]. The magnitude of radial flow is directly influenced by the initial geometry of the collision: events with smaller initial sizes tend to be denser, leading to stronger radial flow [2–4]. This manifests as flatter transverse momentum (p_T) spectra, denoted as $n(p_T)$, and higher average transverse momentum, $\langle p_T \rangle$ (see Fig. 1a). Conversely, larger initial sizes result in weaker radial flow, steeper spectra, and lower $\langle p_T \rangle$ values.

Radial flow fluctuations can be quantitatively assessed through event-by-event (EbE) variations in either $\langle p_T \rangle$, denoted as $\delta[p_T]$, or $n(p_T)$, denoted by $\delta n(p_T)$, where $\delta X = X - \langle X \rangle$ represents the deviation from the event-averaged quantity. These fluctuations are quantified by a p_T integrated observable, $v_0 \equiv \sqrt{\langle (\delta[p_T])^2 \rangle} / \langle [p_T] \rangle$ and a p_T -differential observable $v_0(p_T)$ [5, 6]. Both v_0 and $v_0(p_T)$ are sensitive to initial conditions, as well as medium properties such as the equation of state and viscosities of the QGP. While integrated v_0 measurements have provided valuable insights across various collision energies and systems, the differential nature of $v_0(p_T)$ offers additional diagnostic power. It can differentiate between distinct initial density profiles that might otherwise yield identical $\langle p_T \rangle$ [5], and it offers a unique avenue to probe p_T -dependent influence of transport coefficients like bulk viscosity [7].

In practice, $v_0(p_T)$ is defined as the correlation between the $\langle p_T \rangle$ and the fractional spectra $n(p_T)$ [6, 8–10], formally defined as:

$$v_0(p_T) = \rho(n(p_T), [p_T]) \frac{\sqrt{\langle (\delta n(p_T))^2 \rangle}}{\langle n(p_T) \rangle}, \quad (1)$$

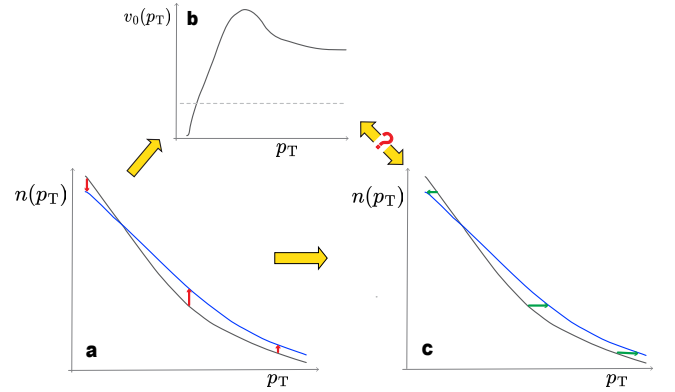


FIG. 1: Cartoon illustration of the momentum rescaling model and its connection to $v_0(p_T)$. (a) Shows the global event-by-event fluctuation of fractional spectra yield, $\delta n(p_T) / \langle n(p_T) \rangle$. The blue curve represents the variation of $n(p_T)$ in an event with large $\langle p_T \rangle$ from the average $\langle n(p_T) \rangle$ represented by the black curve. (b) Illustrates how these fluctuations can be mapped to the characteristic shape of the $v_0(p_T)$ signal [8], which typically rises from negative values, crosses zero, peaks, and then falls. (c) Depicts the core concept of our model: these fluctuations are interpreted as a rescaling of the p_T -axis, $\delta p_T / p_T = g(p_T) \delta[p_T] / \langle [p_T] \rangle$. Our primary goal is to extract this effective p_T -dependent momentum scaling factor, $g(p_T)$, from the experimentally measured $v_0(p_T)$ and average spectrum $\langle n(p_T) \rangle$.

where $\rho(x, y) = \langle \delta x \delta y \rangle / \sqrt{\langle (\delta x)^2 \rangle \langle (\delta y)^2 \rangle}$ is the Pearson correlation coefficient between variables x and y , bounded between -1 and 1. Clearly, $v_0(p_T)$ captures only the component of $n(p_T)$ that correlates with $\langle p_T \rangle$, and is compatible with the following assumption [9]

$$\frac{\delta n(p_T)}{\langle n(p_T) \rangle} = \frac{v_0(p_T)}{v_0} \frac{\delta[p_T]}{\langle [p_T] \rangle}. \quad (2)$$

The first measurement of $v_0(p_T)$ by the ATLAS experiment [8] reveals a characteristic rise-and-fall shape as a function of p_T (see Fig. 1b). This behavior

bears striking similarity to anisotropic flow coefficients $v_n(p_T)$ [11], where the rising portion has been attributed to anisotropic expansion and the falling portion to jet quenching. By analogy, a similar interpretation has been tentatively proposed for $v_0(p_T)$ [8]. However, this interpretation obscures a fundamental question: how much of the observed $v_0(p_T)$ shape arises from the kinematic effect of the varying spectral slope, and how much represents genuine p_T -dependent dynamics beyond global radial flow?

This work addresses this question by introducing a momentum rescaling framework that transforms $v_0(p_T)$ into a more physically transparent observable. The key insight is that radial flow fundamentally boosts particles from lower to higher momentum, as captured in models like the blast-wave parametrization [12, 13]. Event-by-event fluctuations in radial flow can therefore be viewed as a momentum rescaling of the final-state particle spectrum (see Fig. 1c). In this picture, $v_0(p_T)$ factorizes into two distinct components: a kinematic factor determined by the spectral shape, and a dynamical factor $g(p_T)$ that encodes deviations from global momentum rescaling.

This transformation has important implications. We demonstrate that a constant momentum rescaling ($g(p_T) = 1$) already reproduces most features of the measured $v_0(p_T)$, including the rise-and-fall pattern. Deviations of $g(p_T)$ from unity then directly signal additional physics. Most importantly, this framework provides a universal language for theoretical models. Any dynamical model can now make specific predictions for $g(p_T)$ that directly connect to the underlying physics mechanisms.

Momentum rescaling model. We start with the normalized particle spectrum in a single event, $n(p_T)$, with $\int n(p_T) dp_T = 1$. Drawing from hydrodynamic principles, we assume that fluctuations in $n(p_T)$ around the event-averaged spectrum $f(p_T) \equiv \langle n(p_T) \rangle$ are driven by variations in $[p_T]$ around its mean. This scenario corresponds to a rescaling of the momentum axis: $p_T \rightarrow p_T(1 + \delta[p_T]/\langle[p_T]\rangle)$, leading to a transformed spectrum,

$$n(p_T) = \frac{\langle[p_T]\rangle}{[p_T]} f\left(\frac{p_T}{[p_T]} \langle[p_T]\rangle\right), \quad (3)$$

where the prefactor $\langle[p_T]\rangle/[p_T]$ ensures particle number conservation.

For small fluctuations, the spectral variation $\delta n(p_T) = n(p_T) - \langle n(p_T) \rangle$ can be obtained through a first-order Taylor expansion:

$$\frac{\delta n(p_T)}{\langle n(p_T) \rangle} \approx \left. \frac{\partial \ln \langle n \rangle}{\partial \ln [p_T]} \right|_{[p_T] = \langle[p_T]\rangle} \frac{\delta [p_T]}{\langle[p_T]\rangle}. \quad (4)$$

Comparing with Eq. (2) yields our central relation:

$$\frac{v_0(p_T)}{v_0} = \left. \frac{\partial \ln \langle n \rangle}{\partial \ln [p_T]} \right|_{[p_T] = \langle[p_T]\rangle} = -\frac{d \ln \langle n(p_T) \rangle}{d \ln p_T} - 1. \quad (5)$$

The additional -1 term originates from the normalization prefactor in Eq. (3).

This framework implies that under constant fractional momentum rescaling, $v_0(p_T)$ is entirely determined by the spectral shape. For an exponential spectrum characteristic of thermal emission, $\langle n(p_T) \rangle \propto p_T \exp(-2p_T/[p_T])$, we recover $v_0(p_T)/v_0 = 2(p_T/\langle[p_T]\rangle - 1)$ [6]. For a power-law spectrum expected at high p_T region, $\langle n(p_T) \rangle \propto (p_T + p_0)^{-m}$, the result asymptotes to a constant $v_0(p_T)/v_0 = \frac{mp_T}{(p_T + p_0)} - 1 \xrightarrow{p_T \rightarrow \infty} m-1$. The transition of the spectra between these regimes at around $p_T \approx 3-4$ GeV naturally produces a rise-and-fall shape for $v_0(p_T)$.

To capture deviations from global rescaling, we introduce a momentum-dependent factor:

$$\frac{v_0(p_T)}{v_0} = -g(p_T) \left(\frac{d \ln \langle n(p_T) \rangle}{d \ln p_T} + 1 \right), \quad (6)$$

where $g(p_T) = 1$ corresponds to pure global momentum rescaling, and deviations signal additional p_T -dependent dynamics.

Model implementation. The extraction of $g(p_T)$ from experimental measurements proceeds through the following steps:

1. **Baseline calculation:** The first step is to compute the expected $v_0(p_T)$ assuming pure global rescaling using published spectra:

$$\left(\frac{v_0(p_T)}{v_0} \right)_{\text{model}} = -\frac{d \ln \langle n(p_T) \rangle}{d \ln p_T} - 1. \quad (7)$$

2. **Acceptance correction:** ATLAS measurements use reference particles within $p_T \in A = [0.5, 2]$ GeV, yielding v_0^A [8]. The relationship to full-acceptance v_0 is given by [6, 9]:

$$C_A = \frac{v_0^A}{v_0} = \frac{\int_A (p_T - \langle[p_T]\rangle_A) \langle n(p_T) \rangle v_0(p_T) / v_0 dp_T}{\int_A p_T \langle n(p_T) \rangle dp_T}, \quad (8)$$

where $\langle[p_T]\rangle_A$ denotes the mean p_T within range A . This yields:

$$\left(\frac{v_0(p_T)}{v_0^A} \right)_{\text{model}} = -\left(\frac{d \ln \langle n(p_T) \rangle}{d \ln p_T} + 1 \right) / C_A. \quad (9)$$

3. **Incorporate normalization offset:** As demonstrated in previous work, the choice of the reference momentum range A can introduce a global offset in the measured $v_0(p_T)$ [10]. To account for this, a shift is applied to align the zero-crossing points of the model with the experimental data for each centrality class:

$$s = \left(\frac{v_0(p_T^0)}{v_0^A} \right)_{\text{model}} - \left(\frac{v_0(p_T^0)}{v_0^A} \right)_{\text{data}}, \quad (10)$$

where p_T^0 denotes the p_T value at which the ATLAS data crosses zero, i.e. $v_0(p_T^0) = 0$.

4. **Extract $g(p_T)$** : Finally, $g(p_T)$ is determined by taking the ratio of the measured v_0^A and $v_0(p_T)$ data from ATLAS [8] to the offset-corrected model prediction:

$$g(p_T) = \frac{(v_0(p_T)/v_0^A)_{\text{data}}}{-(d \ln \langle n(p_T) \rangle / d \ln p_T + 1) / C_A - s}. \quad (11)$$

This allows for the calculation of the scaled variance of the momentum fluctuation as a function of p_T :

$$\frac{\Delta_{p_T}(p_T)}{p_T} \equiv g(p_T) v_0 = g(p_T) \frac{v_{0,\text{data}}^A}{C_A}. \quad (12)$$

Results. The charged particle spectra used for our study are taken from ALICE [14] and ATLAS [15] collaborations. The spectra data include pp collisions and various centrality classes in Pb+Pb collisions at $\sqrt{s_{NN}} = 5.02$ TeV, spanning from 0.15 GeV to well beyond 100 GeV. The corresponding v_0 and $v_0(p_T)$ data are measured by ATLAS [8].

Figure 2a shows that assuming global rescaling ($g(p_T) = 1$) produces a characteristic pattern in central collisions: an initial rise to $p_T \approx 4$ GeV, followed by a decrease to ~ 10 GeV, then a gradual increase at higher p_T where the spectrum flattens. This rise-and-fall signature weakens progressively in peripheral and pp collisions.

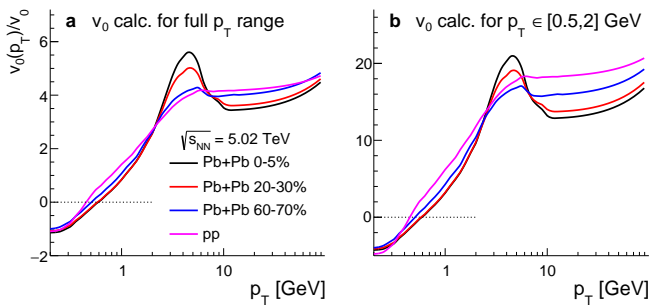


FIG. 2: The $v_0(p_T)/v_0$ (a) and $v_0(p_T)/v_0^A$ (b) calculated from the charged hadron spectra via Eq. (7) and Eq. (9), respectively, assuming a constant fractional momentum rescaling ($g(p_T) = 1$). Results are shown for pp and several central classes in Pb+Pb collisions at $\sqrt{s_{NN}} = 5.02$ TeV.

The acceptance factor C_A for the ATLAS reference range $A = [0.5, 2]$ GeV, calculated via Eq. (8), varies from 0.228 (peripheral) to 0.269 (central) as shown in Appendix A. This centrality dependence arises from the fact that spectra become flatter in more peripheral collisions, which in turn reduces the spread of $v_0(p_T)/v_0^A$ relative to $v_0(p_T)/v_0$.

Figure 3a compares model predictions with ATLAS $v_0(p_T)/v_0^A$ data after zero-crossing alignment. Significant deviations emerge, particularly at intermediate p_T . The extracted $g(p_T)$ (Fig. 3b) reveals systematic departures from unity that are most pronounced in central collisions: starting at $g \sim 0.8$ for low p_T , peaking near 1.4 around 2 GeV, then gradually decreasing to ~ 1.2 at

high p_T . Peripheral collisions show substantially smaller deviations.

These patterns suggest multiple physical origins, including: 1) mass-dependent boost that can not be accounted for by a single $[p_T]$, 2) p_T -dependent viscous corrections that modify the flow profile differently at different momenta, 3) resonance decays and hadronic rescattering that can modify the momentum dependence, or 4) contributions from jet production and jet quenching that generate yield fluctuations not perfectly correlated with the low- p_T radial flow. The centrality dependence indicates these effects strengthen with system size. However, further model investigation are necessary to fully understand the behavior of $g(p_T)$.

Figure 3c presents $\Delta_{p_T}(p_T)/p_T$, quantifying the absolute momentum fluctuation scale. This scaling factor shows a mild p_T dependence but exhibits a significant increase toward more peripheral collisions, a trend that is primarily governed by the centrality-dependent behavior of the integral v_0 .

Prediction at RHIC energy. Given the qualitative success of the global momentum rescaling framework in describing the $v_0(p_T)/v_0$ data, we extend our model to make predictions for the top RHIC energy of $\sqrt{s_{NN}} = 0.2$ TeV. These predictions are based on published spectra data from pp and Au+Au collisions [16, 17]. Figure 4 presents these predictions alongside LHC results for various reference ranges.

The overall trends and magnitudes of the predictions are broadly similar between RHIC and LHC energies. However, a closer inspection reveals several key differences. The predicted values are systematically higher at the lower $\sqrt{s_{NN}}$, which can be partially attributed to the smaller $\langle [p_T] \rangle$ values at RHIC (since $p_T^0 \approx \langle [p_T] \rangle$). A similar trend was also observed in a hydrodynamic simulation [18]. In the higher p_T region (> 2 GeV), the RHIC predictions show a smaller dependence on centrality compared to those at the LHC. Furthermore, for $p_T > 5$ GeV, the RHIC results exhibit a more gradual decrease with increasing p_T than the LHC results. These behaviors can be understood from the fact that for a given p_T , the particle spectra at lower $\sqrt{s_{NN}}$ are steeper. According to Eq. 5, a steeper spectrum tends to produce a larger $v_0(p_T)$ value.

Future extension. The momentum rescaling framework introduced in this work provides a useful tool for characterizing radial flow fluctuations and their connection to QGP dynamics. Two promising extensions for future research are outlined here.

Two-particle radial flow fluctuations. According to Ref. [6], $v_0(p_T)$ can also be measured by correlating multiplicity fluctuations in two different transverse momentum ranges, p_{T1} and p_{T2} ,

$$V_0(p_{T1}, p_{T2}) = \frac{\langle \delta n(p_{T1}) \delta n(p_{T2}) \rangle}{\langle n(p_{T1}) \rangle \langle n(p_{T2}) \rangle}. \quad (13)$$

The collective nature of radial flow implies a factorization: $V_0(p_{T1}, p_{T2}) = v_0(p_{T1})v_0(p_{T2})$. Within the mo-

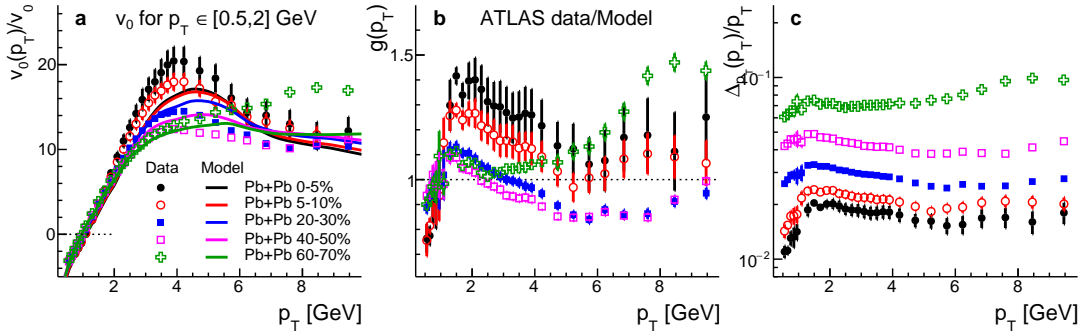


FIG. 3: **Extract physics by comparing with ATLAS $v_0(p_T)$ data.** (a) Shows the calculated $v_0(p_T)/v_0^A$ (solid lines) after applying the zero-crossing shift (Eq. (10)), compared with experimental ATLAS data (markers) for various Pb+Pb centrality classes at $\sqrt{s_{NN}} = 5.02$ TeV. (b) Illustrates the extracted $g(p_T)$ (markers), calculated according to Eq. (11), for the same centrality classes. A dashed line at $g(p_T) = 1$ indicates the global momentum rescaling scenario. (c) Presents the absolute p_T -differential momentum rescaling factor, $\Delta_{p_T}(p_T)/p_T$, as a function of p_T in same centrality classes, calculated using Eq. (12).

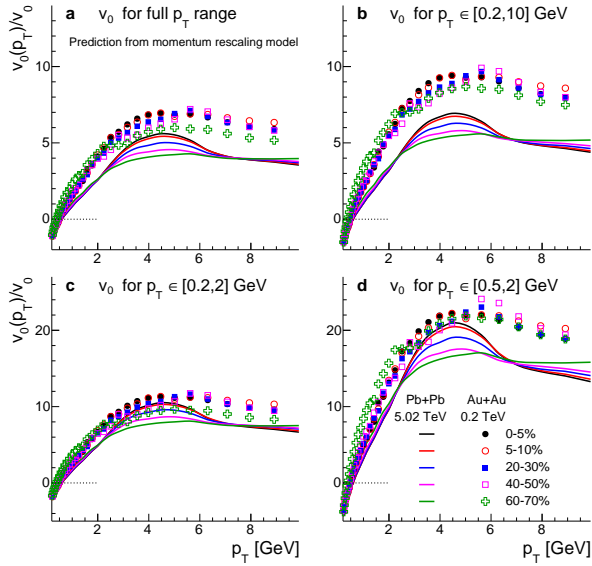


FIG. 4: **Predicted $v_0(p_T)/v_0$ at RHIC and LHC energies based on momentum rescaling model.** The $v_0(p_T)/v_0$ calculated from charged hadron spectra via Eq. (7) for Pb+Pb collisions at $\sqrt{s_{NN}} = 5.02$ TeV (solid lines, LHC) and Au+Au collisions at $\sqrt{s_{NN}} = 0.2$ TeV (markers, RHIC). Panels show results normalized to v_0 calculated in different reference p_T ranges: (a) full p_T range, (b) $0.2 < p_T < 10$ GeV range, (c) $0.2 < p_T < 2$ GeV range, and (d) $0.5 < p_T < 2$ GeV range.

mentum rescaling model, this leads to the prediction (Eq. (4)):

$$V_0(p_{T1}, p_{T2}) \approx \left(\frac{d \ln \langle n \rangle}{d \ln p_T}(p_{T1}) + 1 \right) \left(\frac{d \ln \langle n \rangle}{d \ln p_T}(p_{T2}) + 1 \right). \quad (14)$$

Deviations from this prediction would signal momentum-dependent decorrelation effects arising from subleading flow [5].

High-order radial flow fluctuations. The momentum rescaling model can be extended to investigate higher-order spectral fluctuations, such as the skewness, $v_0\{3\}(p_T)$, and kurtosis $v_0\{4\}(p_T)$ of the spectra fluctu-

ations [10]:

$$\begin{aligned} v_0\{3\}(p_T)^3 &= \langle (\delta n(p_T))^3 \rangle / \langle n(p_T) \rangle^3, \\ v_0\{4\}(p_T)^4 &= \frac{\langle (\delta n(p_T))^4 \rangle - 3 \langle (\delta n(p_T))^2 \rangle^2}{\langle n(p_T) \rangle^4}, \\ &\dots \end{aligned} \quad (15)$$

Based on Eq. (4), in the limit of global rescaling, all high-order fluctuations are expected to exhibit the same p_T dependence as the variance:

$$\frac{v_0\{k\}(p_T)}{v_0\{k\}} \approx - \frac{d \ln \langle n(p_T) \rangle}{d \ln p_T} - 1. \quad (16)$$

This can be further extended to the case where each particle in a k -particle multiplet is selected from a different p_T range:

$$V_0\{k\}(p_{T1}, p_{T2}, \dots) \approx \prod_{i=1}^k \left(- \frac{d \ln \langle n \rangle}{d \ln p_T}(p_{Ti}) - 1 \right). \quad (17)$$

Summary and outlook. We have introduced a new approach to understanding radial flow fluctuations by recasting $v_0(p_T)$ as a momentum rescaling function $g(p_T)$. This framework reveals that the characteristic rise-and-fall pattern of $v_0(p_T)$ is primarily a kinematic effect from the varying spectral slope: a constant rescaling ($g(p_T) = 1$) already captures the essential features.

The transformation $v_0(p_T) \rightarrow g(p_T)$ separates kinematic from dynamical effects. Analysis of ATLAS data at $\sqrt{s_{NN}} = 5.02$ TeV reveals that $g(p_T)$ deviates from unity by about 20–40%: suppression at low p_T ($g(p_T) \sim 0.8$), enhancement at intermediate p_T ($g(p_T) \sim 1.4$), and gradual decrease at high p_T . These deviations are largest in central collisions and systematically decrease toward peripheral collisions, revealing their connection to specific effects in the QGP.

The $g(p_T)$ is an observable more suitable for theoretical interpretation: any dynamical model can now make specific predictions for $g(p_T)$ that directly encode its physics content. Our predictions for RHIC energies suggest that spectral shape differences alone can generate

significant energy-dependent features, providing a clear baseline for future measurements to identify genuine dynamical effects.

This momentum rescaling principle opens new avenues for experiment and theory. Future measurements of $g(p_T)$ for identified particles will test flow universality and reveal mass effects. Calculating $g(p_T)$ within blast-wave parameterizations, viscous hydrodynamics, and models including jet quenching will provide quantitative tests of QGP dynamics. The framework extends naturally to higher-order fluctuations, where deviations from factorization signal p_T -dependent non-Gaussian dynamics. This approach may also apply to anisotropic flow $v_n(p_T)$, where $v_n(p_T)$ could potentially be understood through azimuthally-dependent momentum rescaling. This approach could then be used to explore the correlation between anisotropic flow and radial flow $\langle v_n(p_T)^2 v_0(p_T) \rangle$ [19] within the momentum rescaling framework. This connection between isotropic and anisotropic collective phenomena warrants future investigation.

This work is supported by DOE Research Grant Number DE-SC0024602. The author acknowledges valuable discussions with Derek Teaney, Somadutta Bhatta, Zhengxi Yan, and Giuliano Giacalone.

Appendix

A. Relating the integral v_0 in different p_T ranges

The experimental determination of $v_0 = \sqrt{\langle (\delta[p_T])^2 \rangle} / \langle [p_T] \rangle$ varies across experiments due to different detector acceptances and analysis strategies. STAR and ALICE typically use $p_T > 0.2$ GeV, CMS employs $p_T > 0.3$ GeV, while ATLAS uses $p_T > 0.5$ GeV. Though these measurements probe the same underlying radial flow fluctuations, their numerical values differ substantially due to the p_T -range dependence.

To quantify this effect, we employ the acceptance factor C_A introduced in Ref. [9], which relates measurements within a specific range $p_T \in A = [p_T^{\min}, p_T^{\max}]$ to the full-acceptance value through Eq. (8). This factor encodes how the interplay between spectral shape and $v_0(p_T)$ weights different momentum regions.

Figure 5 presents our predictions for C_A as a function of acceptance boundaries. Several key features emerge: 1) C_A decreases in peripheral collisions for larger p_T^{\max} , reflecting their flatter spectra. 2) RHIC shows systematically larger C_A than LHC due to steeper spectra at lower energies. 3) The acceptance factor saturates for $p_T^{\max} > 5$ –6 GeV at LHC but earlier (~ 3 –4 GeV) at RHIC.

These trends arise because C_A weights contributions from both the local yield $\langle n(p_T) \rangle$ and the local $v_0(p_T)$ value (Eq. (8)). In peripheral collisions, the flatter spectrum reduces the relative contribution from low- p_T particles where $v_0(p_T)$ is negative, thereby decreasing C_A .

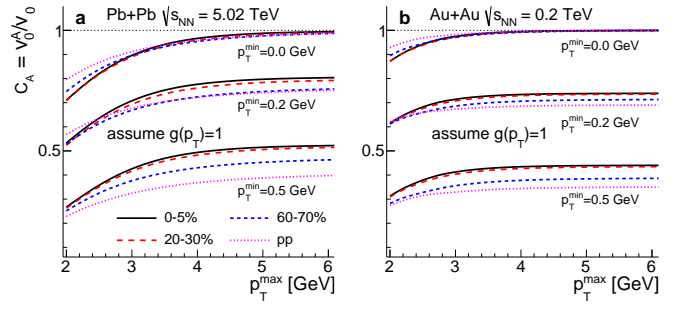


FIG. 5: **Acceptance factor** $C_A(p_T^{\min}, p_T^{\max})$. The acceptance factor $C_A = v_0^A / v_0$ (defined in Eq. (8)) is shown as a function of p_T^{\max} for different values of p_T^{\min} (as labeled for each group of curves). Results are shown for Pb+Pb collisions at $\sqrt{s_{NN}} = 5.02$ TeV (a) and Au+Au collisions at $\sqrt{s_{NN}} = 0.2$ TeV (b). Each group of curves consists of results for four centrality classes.

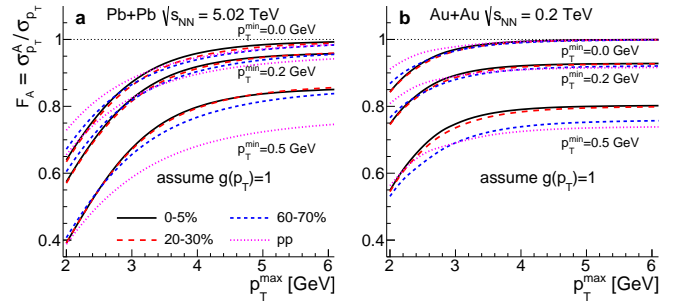


FIG. 6: **Fraction of momentum fluctuation** $F_A(p_T^{\min}, p_T^{\max})$. The variance fraction F_A (Eq. (18)), representing how momentum fluctuations are distributed across p_T , is shown as a function of p_T^{\max} for different values of p_T^{\min} (as labeled for each group of curves). Results are shown for Pb+Pb collisions at $\sqrt{s_{NN}} = 5.02$ TeV (a) and Au+Au collisions at $\sqrt{s_{NN}} = 0.2$ TeV (b). Each group of curves consists of results for four centrality classes.

A disadvantage of v_0 is its strong dependence on $\langle [p_T] \rangle$, which itself varies considerably with the choice of p_T range. Hence, we introduce a complementary observable that removes the $\langle [p_T] \rangle$ dependence:

$$F_A = C_A \frac{\langle [p_T] \rangle}{\langle [p_T] \rangle_A} = \frac{\sqrt{\langle (\delta[p_T])^2 \rangle_A}}{\sqrt{\langle (\delta[p_T])^2 \rangle}}. \quad (18)$$

This quantity directly measures the fraction of total momentum variance contained within range A .

Figure 6 reveals that F_A is substantially larger than C_A and is also greater at lower $\sqrt{s_{NN}}$. The reference range $0.5 < p_T < 2$ GeV captures approximately 40% of total fluctuations at LHC but 55% at RHIC, reflecting the concentration of particle production at lower momenta for smaller $\sqrt{s_{NN}}$. The saturation behavior of F_A with p_T^{\max} provides a direct measure of the momentum reach of collective radial flow. This influence extends to 5–6 GeV at LHC but only 3–4 GeV at RHIC.

B. Dependence of $v_0(p_T)/v_0$ on magnitude of momentum fluctuation

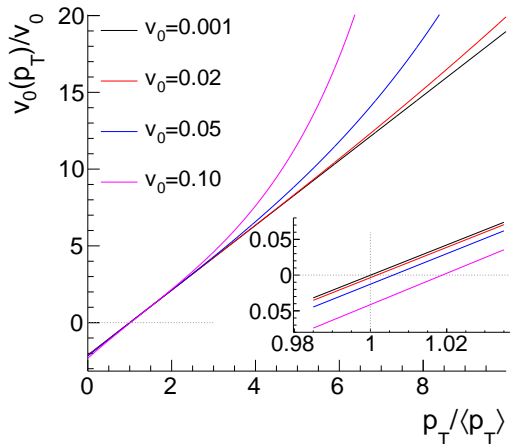


FIG. 7: **Breakdown of linear approximation for large fluctuations.** Exact calculation of $v_0(p_T)/v_0$ for exponential spectra reveals systematic deviations from the linear prediction (Eq. (20)) as v_0 increases. The zero-crossing shift (inset) and shape distortions become significant for $v_0 > 0.05$, indicating breakdown of Eq. (5) and the need for nonlinear corrections in peripheral collisions and small systems.

The formula used to predict $v_0(p_T)$, Eq. (5), is derived under the assumption of small momentum fluctuations with leading-order Taylor expansion. This approximation may break down for large values of v_0 , which are relevant for peripheral collisions and small systems. To illustrate this limitation and establish the validity range of our approach, we consider an exponential spectrum:

$$\langle n(p_T) \rangle \propto \frac{p_T}{[p_T]^2} \exp\left(-\frac{2p_T}{[p_T]}\right). \quad (19)$$

For this spectrum, the exact result for small v_0 is [6]:

$$v_0(p_T) = 2v_0 \left(\frac{p_T}{\langle [p_T] \rangle} - 1 \right). \quad (20)$$

Experimental measurements span a wide range of v_0 values. In Au+Au (RHIC) [20–22] and Pb+Pb (LHC) [4, 23], v_0 ranges from ~ 0.01 (central) to > 0.05 (peripheral). Small systems show even larger values: 0.05–0.14 in pp collisions [23]. These values are generally larger at RHIC energies [21], primarily due to their smaller $\langle [p_T] \rangle$ values. Crucially, most measurements use restricted p_T ranges (typically 0.2–2 GeV). Full-acceptance values could be factor ~ 2 larger (see Fig. 5). This implies that the total v_0 in Au+Au or Pb+Pb collisions could reach values as high as 0.02 in central, 0.05 in mid-central, and greater than 0.1 in peripheral collisions.

Figure 7 quantifies deviations from the linear approximation (Eq. (20)) for different magnitudes of v_0 . Key findings are:

- For $v_0 \lesssim 0.02$ (typical of central collisions): deviations remain below 5%.
- For $v_0 = 0.05$ (mid-peripheral): 10% deviations appear at $p_T \sim 4$ GeV.
- For $v_0 = 0.1$ (peripheral/small systems): deviations reach 40% at high p_T .
- The zero-crossing point shifts systematically to larger p_T with increasing v_0 .

These results have important implications:

- The linear framework remains accurate for central and mid-central collisions ($v_0 \lesssim 0.05$).
- Peripheral collisions require nonlinear corrections, particularly at high p_T .
- In extreme cases ($v_0 > 0.1$), the same spectrum can produce qualitatively different $v_0(p_T)/v_0$ shapes purely from the magnitude of fluctuations.

To handle large-fluctuation regimes accurately, future work should develop systematic expansions or numerical approaches for a proper interpretation of $v_0(p_T)$. This is particularly important for small systems where collective behavior remains debated.

-
- [1] U. Heinz and R. Snellings, *Ann. Rev. Nucl. Part. Sci.* **63**, 123 (2013), [arXiv:1301.2826 \[nucl-th\]](#).
 - [2] P. Bozek and W. Broniowski, *Phys. Rev. C* **85**, 044910 (2012), [arXiv:1203.1810 \[nucl-th\]](#).
 - [3] G. Giacalone, F. G. Gardim, J. Noronha-Hostler, and J.-Y. Ollitrault, *Phys. Rev. C* **103**, 024909 (2021), [arXiv:2004.01765 \[nucl-th\]](#).
 - [4] ATLAS Collaboration, *Phys. Rev. Lett.* **133**, 252301 (2024), [arXiv:2407.06413 \[nucl-ex\]](#).
 - [5] A. Mazeliauskas and D. Teaney, *Phys. Rev. C* **93**, 024913 (2016), [arXiv:1509.07492 \[nucl-th\]](#).
 - [6] B. Schenke, C. Shen, and D. Teaney, *Phys. Rev. C* **102**, 034905 (2020), [arXiv:2004.00690 \[nucl-th\]](#).
 - [7] R. Samanta, S. Bhatta, J. Jia, M. Luzum, and J.-Y. Ollitrault, *Phys. Rev. C* **109**, L051902 (2024), [arXiv:2303.15323 \[nucl-th\]](#).
 - [8] G. Aad *et al.* (ATLAS), (2025), [arXiv:2503.24125 \[nucl-ex\]](#).
 - [9] T. Parida, R. Samanta, and J.-Y. Ollitrault, *Phys. Lett. B* **857**, 138985 (2024), [arXiv:2407.17313 \[nucl-th\]](#).
 - [10] S. Bhatta, A. Dimri, and J. Jia, (2025), [arXiv:2504.20008 \[nucl-th\]](#).
 - [11] ATLAS Collaboration, *Phys. Rev. C* **86**, 014907 (2012), [arXiv:1203.3087 \[hep-ex\]](#).

- [12] E. Schnedermann, J. Sollfrank, and U. W. Heinz, *Phys. Rev. C* **48**, 2462 (1993), [arXiv:nucl-th/9307020](#) .
- [13] F. Retiere and M. A. Lisa, *Phys. Rev. C* **70**, 044907 (2004), [arXiv:nucl-th/0312024](#) .
- [14] S. Acharya *et al.* (ALICE), *JHEP* **11**, 013 (2018), [arXiv:1802.09145 \[nucl-ex\]](#) .
- [15] G. Aad *et al.* (ATLAS), *JHEP* **07**, 074 (2023), [arXiv:2211.15257 \[hep-ex\]](#) .
- [16] J. Adams *et al.* (STAR), *Phys. Rev. Lett.* **91**, 172302 (2003), [arXiv:nucl-ex/0305015](#) .
- [17] S. S. Adler *et al.* (PHENIX), *Phys. Rev. C* **69**, 034910 (2004), [arXiv:nucl-ex/0308006](#) .
- [18] S. A. Jahan, H. Roch, and C. Shen, (2025), [arXiv:2507.11394 \[nucl-th\]](#) .
- [19] T. Parida, R. Samanta, and J.-Y. Ollitrault, *Phys. Lett. B* **868**, 139729 (2025), [arXiv:2506.18690 \[nucl-th\]](#) .
- [20] J. Adams *et al.* (STAR), *Phys. Rev. C* **72**, 044902 (2005), [arXiv:nucl-ex/0504031](#) .
- [21] J. Adam *et al.* (STAR), *Phys. Rev. C* **99**, 044918 (2019), [arXiv:1901.00837 \[nucl-ex\]](#) .
- [22] M. I. Abdulhamid *et al.* (STAR), *Nature* **635**, 67 (2024), [arXiv:2401.06625 \[nucl-ex\]](#) .
- [23] ALICE Collaboration, *Eur. Phys. J. C* **74**, 3077 (2014), [arXiv:1407.5530 \[nucl-ex\]](#) .